

HILL-SHADING BASED ON ANISOTROPIC DIFFUSE ILLUMINATION

Klemen ZAKŠEK¹², Krištof OŠTIR¹³, Peter PEHANI¹³, Žiga KOKALJ¹³, Ekkehard POLERT⁴

¹Centre of Excellence Space-Si, Aškerčeva 12, SI-1000 Ljubljana, Slovenia

²Institute of Geophysics, University of Hamburg, Bundesstr. 55, D-20146 Hamburg, Germany

klemen.zaksek@zmaw.de

³Institute of Anthropological and Spatial Studies, ZRC SAZU, Novi trg 2, SI-1000 Ljubljana, Slovenia

kristof@zrc-sazu.si (K.O.), peter.pehani@zrc-sazu.si (P.P.), ziga.kokalj@zrc-sazu.si (Ž.K.)

⁴Retired, Hamburg, Germany

d.dreysacz@arcor.de

Abstract

Analytical hill-shading is a computer-based process of generating a shaded surface from a digital surface model. There are numerous analytical hill-shading techniques; however only the method based on the cosine of the incidence angle of an imaginative direct illumination source became a standard feature in most GIS software. Although widely accepted, this method has two major drawbacks: identifying details in deep shades and inability to properly represent linear features lying parallel to the light beam. Several authors have tried to overcome these limitations by changing the position of the light source.

Our contribution explores alternative terrain visualization techniques based on diffuse, rather than direct, illumination. We first compare three published methods for terrain visualization based on diffuse illumination: openness [16], sky-view factor [17], and uniform sky illumination [9]. These are all based on assumption that illumination is isotropic – the brightness of the light source is direction independent. This visualizes the concave surface forms as dark regions and convex surface forms as bright features. Therefore, these three methods give better insight on the relative elevation of each point than the classical analytical hill-shading.

Yet the analytical hill-shading seems to be more intuitive for most users. Thus we upgraded the previous studies on diffuse surface illumination – instead of considering an isotropically bright sky as the light source we tested various sky brightness distributions. The results can be used as a general terrain visualization because the method combines advantages of direct and diffuse light sources. In particular, we show that such a visualization improves the recognition of local scale features on high resolution DEMs, which is very important in different applications: visual inspection of DEM, recognition of archaeological features, etc.

Keywords: hill-shading, diffuse illumination, sky-view factor, anisotropic sky brightness, terrain

1. INTRODUCTION

Development of GIS software made analytical hill-shading one of the most common methods for terrain visualization. Analytical hill-shading is a computer-based process of generating a shaded relief from a raster digital elevation model (DEM). It is a description of how the relief surface reflects the incoming illumination based on physical laws or empirical knowledge. There are numerous analytical hill-shading techniques [5], however only the method developed by Yoëli [15] became a standard feature in common GIS software. Therefore, when we speak about analytical hill-shading (SHD) we consider his method. The computed gray value of the classical SHD is proportional to the cosine of the illumination incidence angle on the relief surface. The method is fast and its results are intuitive to interpret, however it also has two major drawbacks. Direct illumination restricts the visualization in dark shades and very brightly lit areas, where no or very little detail can be perceived. A single light beam also fails to unveil linear structures that lie parallel to it [1].

Another approach to visualize the terrain is employing the uniform diffuse illumination. Diffuse illumination was systematically studied in the field of computer graphics (video games, photorealistic rendering) already in the 1990s when Zhukov et al. [18] introduced obscurances. Because diffuse illumination requires long processing time some studies aimed to simplify it. Proxies for such an illumination model can be extracted from SHD from multiple directions: mean of multiple shading from different azimuths [4], combination of standard SHD (azimuth 315°) with vertical illumination [7], RGB image from hill-shades from three different directions [1, 3]. More advanced methods are based on the horizon estimation. Yokoyama et al. [16] described openness (OPN) – a method that is based on estimating the mean horizon elevation angle in eight directions within a defined search radius. Zakšek et al. [17] proposed to use sky-view factor (SVF) which is a solid angle of the visible sky hemisphere obscured by the terrain. Kennelly and Stewart [9] considered Lambertian reflection while using a uniform sky illumination (USI) instead of point source illumination.

Such approaches significantly enhance perception of relative elevation but they lack the ease of reading the results for non GIS experts. A logical step is merging classical SHD with one of the mentioned methods [9, 16, 17]. In this paper we propose to use an anisotropic diffuse illumination that has advantages of classical SHD and the previously cited methods: it provides the intuitive perception of the terrain, it produces sharper images than the classical SHD (for instance the ridges are easier to follow), even subtle features are easy to detect, etc. In the following, we therefore shortly compare some existing methods based on diffuse illumination (chapter 2) and extend them by considering anisotropic diffuse illumination. We propose two simple solutions for generating anisotropic diffuse illumination source (chapter 3). Before the conclusion we discuss the proposed methods and compare them to SHD and SVF (chapter 4).

2. TERRAIN VISUALIZATION USING ISOTROPIC DIFFUSE ILLUMINATION

OPN [16], SVF [17], and USI [9] have their origin in a horizon determination (fig. 1), thus their results are similar (fig. 2). There is, however a significant geometric difference between the OPN and the other two methods. OPN does not limit the estimation of each horizon elevation angle (γ) with the mathematical horizon as other two methods do. In other words, OPN considers the whole sphere and not only the celestial hemisphere like SVF and USI. Therefore, the maximum OPN value can be greater than $\pi/2$. In addition, interpreting OPN is sometimes difficult because a slope is visualized in the same manner as a horizontal plane (both a long slope and a horizontal plane without any obstacles have an openness of $\pi/2$). Using an appropriate histogram stretch, it is possible to visualize OPN in a similar way as SVF or USI, but only in the concave areas (with horizon zenith angles in all search directions less than $\pi/2$). In other areas, OPN gives significantly different results. We can therefore conclude that OPN is not as intuitive as SVF or USI, but it is more appropriate in automatic detection of linear structures because the method exposes many edges.

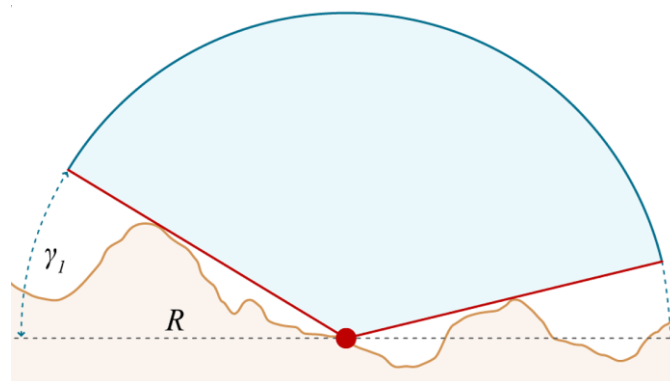


Fig. 1. For each direction i the methods OPN, SVF, and USI search for the horizon elevation angle γ_i within the vicinity of a stand-point (red dot) limited by the radius R . The blue line represents the visible sky (limited by terrain) that illuminates the stand-point. Since the isotropic illumination is assumed, the brightness of the sky is direction independent.

There are also further differences between these methods. OPN merely averages the horizon elevation angle in n (usually 8) directions (eq. 1). SVF estimates the solid angle of the visible sky in each direction; then it averages the solid angles and normalizes the mean value with the solid angle of a hemisphere (eq. 2).

$$\text{OPN} = \frac{\sum_{i=1}^n \gamma_i}{n} \quad (1)$$

$$\text{SVF} = 1 - \frac{\sum_{i=1}^n \sin \gamma_i}{n} \quad (2)$$

OPN and SVF therefore merely provide information about the illumination availability. They estimate how much of the whole available light source can be used to illuminate the terrain. They do not, however, provide any information about the interaction of the illumination with the terrain surface. This is what USI does – it assumes that the terrain is perfectly matte – a Lambertian surface, where is the reflected light intensity a function of the cosine of illumination incidence angle δ . The brightness of the Lambertian surface is independent of the viewing angle. USI therefore integrates the cosine of incidence angle from each infinitesimal solid angle of the visible sky (eq. 3).

$$\text{USI} = \frac{1}{2\pi} \cdot \sum_{i=1}^n \left[\frac{2\pi}{n} \cos \varepsilon \left(\frac{\pi}{2} \sin \delta - s \cos \delta \cos^2 \gamma_i - \sin \delta \sin \gamma_i \cos \gamma_i - \gamma_i \sin \delta \right) \right] \quad (3)$$

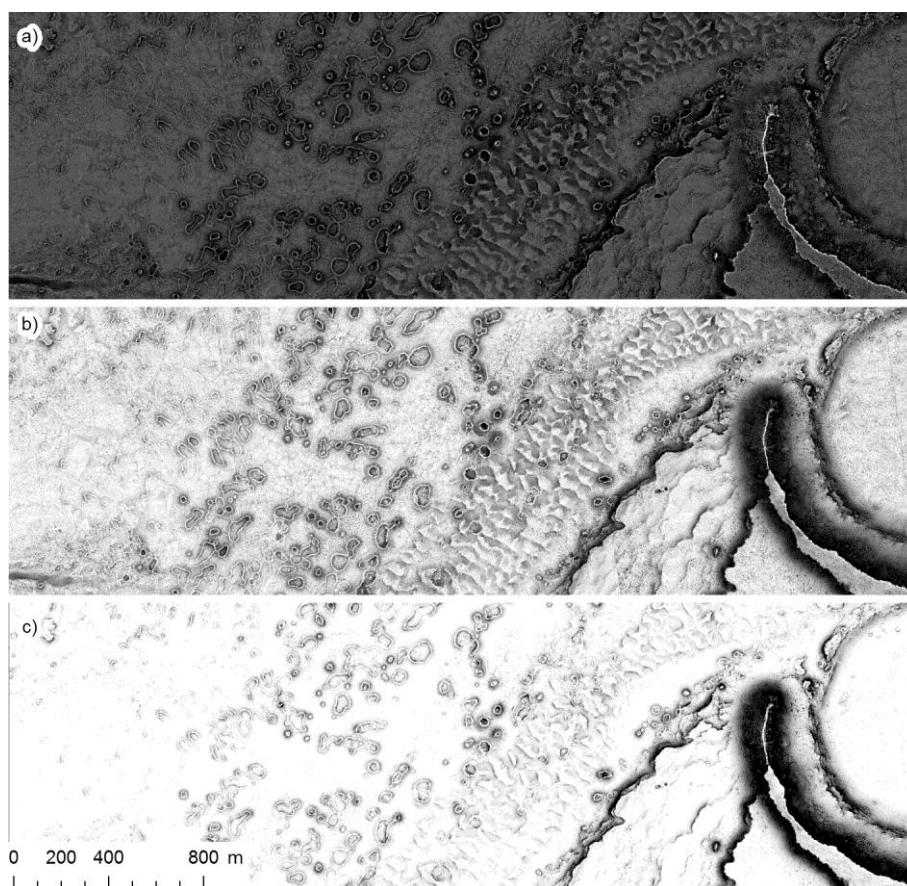


Fig. 2. An example for OPN (a) with linear stretch between -10° and 10° , SVF (b) with linear stretch between 0.7 and 1.0, and USI (c) with linear stretch between 0.85 and 1.0. The image shows ring and cone structures, and dunes in Athabasca Valles, Mars (area of 3800×1200 m; data from HiRISE instrument aboard Mars Reconnaissance Orbiter [10]; credits to NASA/JPL/University of Arizona). All data were processed in 8 directions with the maximum radius of 10 pixels (30 m).

Because of the OPN's limitations that originate in considering the whole hemisphere we do not consider OPN any further (fig. 2). Linear histogram stretch gives USI a smoother looking surface (fig. 2) but SVF is easier and much faster to compute and exposes more details. In the following text we therefore only consider SVF as a representative technique to try with anisotropic diffuse illumination.

3. HILL-SHADING TERRAIN FROM ANISOTROPIC DIFFUSE ILLUMINATION SOURCE

The published methods OPN [16], SVF [17], and USI [9] assume that the intensity of the light source is direction independent. In the field of solar radiation, many methods have been developed that account for anisotropic sky brightness [2, 6, 11, 12, 14]. They claim that the light intensity of each sky element depends on the zenith distance of the sky element and the distance (arc distance across the celestial hemisphere) from the sun. For the visualization purposes we do not need to follow the physical models completely. To enhance the perception of the terrain using diffuse illumination we can simplify to the statement that illumination is azimuth dependent. We thus provide two simple enhancements for SVF based visualization.

Azimuth dependent diffuse illumination source

Azimuth dependent illumination source is the easiest way to account for anisotropy in the sky brightness distribution. Assuming that the sky is brighter in some directions than in others, we can redefine SVF into SVF_a (equation 4). Please note that such an illumination could theoretically lead to problems on the celestial pole – there each azimuth has different weight.

$$SVF_a = 1 - \frac{\sum_{i=1}^n (\sin \gamma_i \cdot p_i)}{\sum_{i=1}^n p_i} \quad (4)$$

where p_i is the weight defined in the equation 5. We propose the weight to be based on the cosine function of half angle. The function exponent c has to be an even number (for instance 2 or 4); the higher it is the larger is anisotropy. The two parameters that have to be set for estimation of the weights are: the azimuth of the highest weight λ_{max} , and the minimal possible weight p_{min} (it is reached when the azimuth is opposite to α_{max}). Theoretically, the p_{min} has values between 0 and 1. If it is set to 0 then the terrain is not illuminated from the direction opposite to α_{max} . If it is set to 1 then the sky brightness is isotropic. An example for such a weight definition is shown in fig. 3.

$$p_i = (1 - p_{min}) \cdot \cos^c \frac{\lambda_i - \lambda_{max}}{2} + p_{min} \quad (5)$$

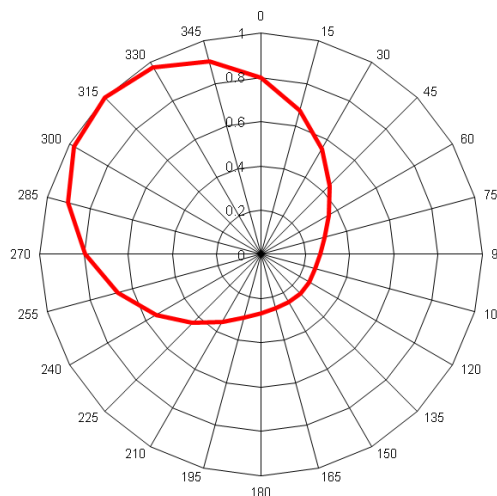


Fig. 3. An example of azimuth weight distribution; the largest weight (1.0) is reached at azimuth of 315°, and the lowest (0.25) at the azimuth of 135°; the cosine function exponent c is set to 4.

According to our experience the optimal setup for the weight parameters are: $c = 4$, $\lambda_{\max} = 315^\circ$, and $0.2 < p_{\min} < 0.5$. Fig. 4 compares the classical SHD, SVF, and SVF_a for the area of Ngorongoro (Tanzania). The obvious difference between the classical SHD and the other two visualisations is larger contrast in the latter two. SVF_a also gives the reader a more intuitive perception of the terrain than the basic SVF. This is evident especially in the lower right corner where a hilly region is much more plastic in SVF_a than in SVF. When compared to the classical SHD, SVF_a preserves the advantages of basic SVF: it gives much more detail in the flat terrain and it “sharpens” the ridges. This enhances especially the perception of the round features (for instance the caldera in the left upper corner).

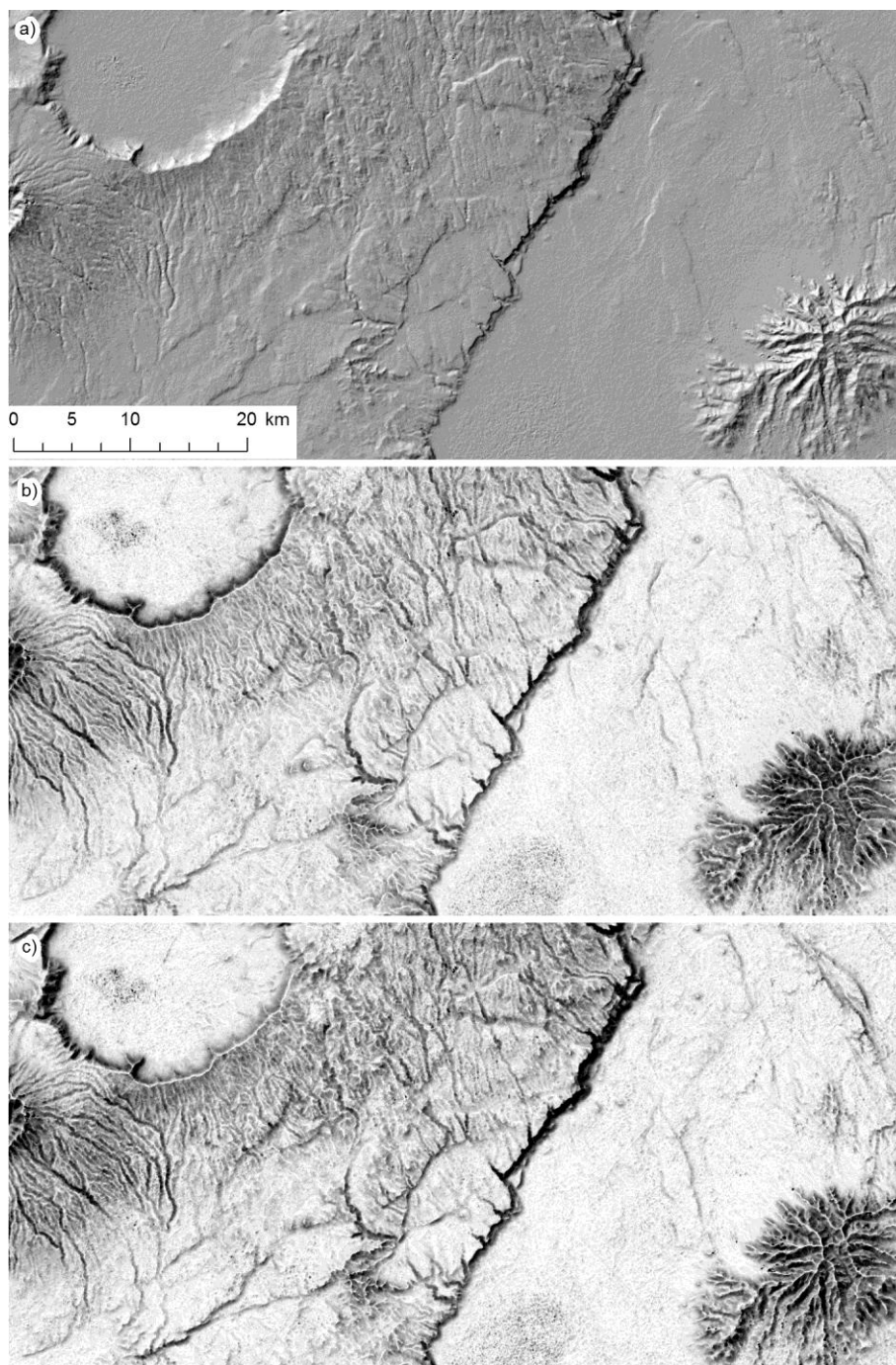


Fig. 4. An example for classical SHD (a), with linear stretch between 0.0 and 1.0, SVF (b) with linear stretch between 0.7 and 1.0, and SVF_a (c) with linear stretch between 0.7 and 1.0. The image shows Ngorongoro crater and its surrounding area in Tanzania (area of 72×36 km; the source of data is ASTER GDEM data [13] obtained from <http://lpdaac.usgs.gov>, maintained by the NASA). SVF and SVF_a were processed in 8 directions with the maximum radius of 10 pixels (300 m).

Solar distance dependent diffuse illumination source

From the physical point of view solar distance dependent illumination source has a more reasonable sky brightness distribution than azimuth dependent illumination source. We assume that the sky is the brightest around the position of the sun. In addition, we assume that the sun is so small that we can shade its direct illumination of the terrain. If the scattering in the atmosphere is direction independent, then the sky brightness depends merely on the arc distance (across the celestial sky) from the sun to the sky element. The easiest way to compute the arc distance is the dot product of unit vectors pointing from the stand point to the sun and from the stand point to the sky element; this gives us the cosine of the arc distance. We redefine SVF into solar distance dependent SVF_d in the equation 6.

$$SVF_d = \int_{VS} f(d_{S-\Omega}) d\Omega \quad (6)$$

An appropriate function f is an exponential function (equation 7). We manipulate the visualization with four parameters. The first two define the solar position: solar elevation angle φ_S , and solar longitude λ_S . For the sky element that covers the position of the sun we set the weight to 1. The most distant sky element receives a predefined minimal weight p_{min} . This can range between 0 and 1 (in the latter case the illumination is isotropic). The decrease of the function value from 1 to p_{min} depends on the exponent c .

$$f(d_{S-\Omega}) = \frac{[\max(d_{S-\Omega}) - d_{S-\Omega}]^c + w_{min}}{[\max(d_{S-\Omega})]^c + w_{min}} \quad (7)$$

$$w_{min} = \frac{[\max(d_{S-\Omega})]^c \cdot p_{min}}{1 - p_{min}}$$

$$d_{S-\Omega} = \arccos([\cos\varphi_S \cos\lambda_S, \cos\varphi_S \sin\lambda_S, \sin\varphi_S] \cdot [\cos\varphi_\Omega \cos\lambda_\Omega, \cos\varphi_\Omega \sin\lambda_\Omega, \sin\varphi_\Omega])$$

In the equation 6 we integrate the product of the function f of the arc distance between the sun and to the sky element $d_{S-\Omega}$ with the area of the corresponding sky element $d\Omega$ over the visible sky VS . We solve this integral numerically by generating a look up table (LUT) where each sky element (with spherical coordinate $\varphi_\Omega, \lambda_\Omega$) has an assigned value SVF_d value. We divide the whole hemisphere in longitude (λ) direction into predefined number of lunes where each lune corresponds to one horizon search direction. Each lune is in the latitude direction separated by the previously chosen resolution. For each sky element we then compute the arc distance from the sun (fig. 5 above). This is the basis to estimate a brightness weight for this element. Then we multiply the computed arc distance by the area of the sky element. Summing all these values from zenith to each tangent gives us a look up table (LUT) that is used to solve equation 6 (an example fig. 5 below).

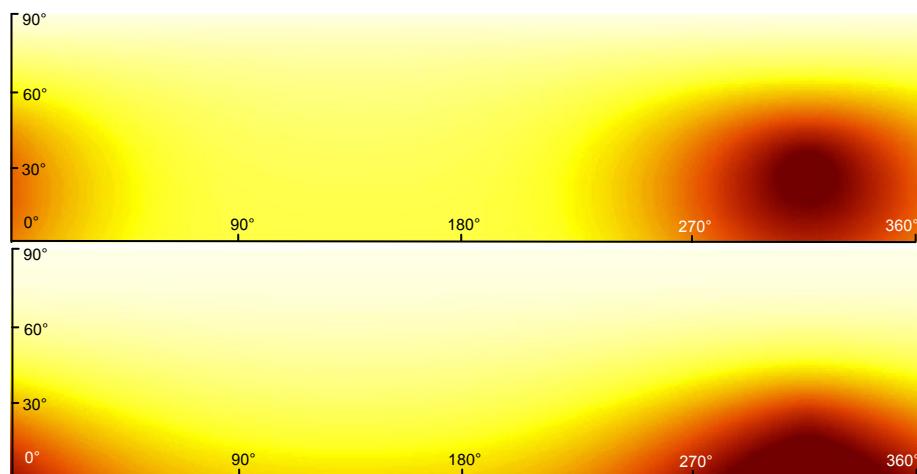


Fig. 5. An example of the visualized weight (according to spherical longitude on x axis and spherical latitude on y axis) based on the arc distance between the sun and the sky element (above) and the final LUT (below). The dark colour represents higher values and bright colour lower values. Parameters were set to:

$$\varphi_S = 30^\circ, \lambda_S = 315^\circ, p_{min} = 0.2, \text{ and } c = 3.$$

Instead of presenting another high resolution example we decided to show that the described procedure works successfully also on low resolution data (200 m); fig. 6 compares the classical SHD, SVF, and SVF_d for the area of the South-Eastern Alps (in Austria and Slovenia). As in fig. 4 we can observe larger contrast in SVF and SVF_d than in the classical SHD. SVF_d was computed using intense illumination anisotropy: $\varphi_S = 10^\circ$, $\lambda_S = 315^\circ$, $p_{\min} = 0.0$, and $c = 9$. Such a setup gives the reader a very plastic perception of the terrain. This is evident especially in the high mountains region. No significant improvement comparing to basic SVF can be observed in the flat regions. The disadvantages of such a strong anisotropy are dark shades in the Alpine region. The classic SHD also reveals a very similar problem.

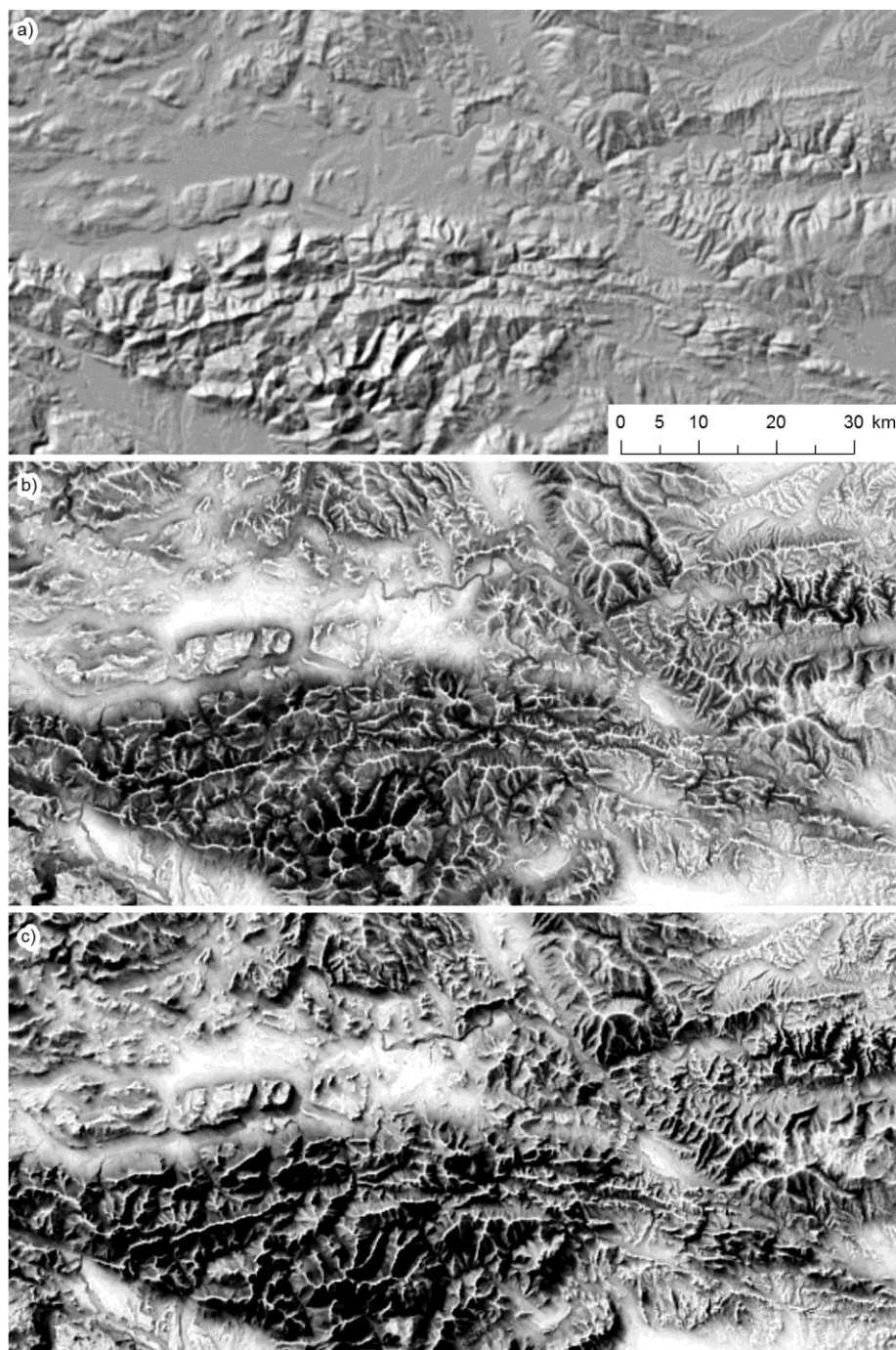


Fig. 6. An example for classical SHD (a) with linear stretch between 0.0 and 1.0, SVF (b) with linear stretch between 0.7 and 1.0, and SVF_d (c) with linear stretch between 0.7 and 1.0. The image shows the South-Eastern Alps in Austria and Slovenia (area of 110 × 55 km; the source of data is SRTM data [8] resampled to 200 m resolution). SVF and SVF_d were processed in 8 directions with the maximum radius of 10 pixels (2000 m). The anisotropy parameters were set to: $\varphi_S = 10^\circ$, $\lambda_S = 315^\circ$, $p_{\min} = 0.0$, and $c = 9$.

4. DISCUSSION AND CONCLUSION

Fig. 7 compares all discussed terrain visualization methods: the classical SHD, SVF, SVF_a , and SVF_d for the karst terrain in South-West Slovenia. To make the comparison easier we chose the azimuth of the directional light $\lambda_S = 315^\circ$ (SHD, SVF_a , SVF_d), elevation of directional light 45° (SHD, SVF_d), exponential coefficient $c = 4$ (SVF_a , SVF_d), and minimum weight $p_{\min} = 0.2$ (SVF_a , SVF_d). The dolines (karstic sinkholes) in lower left corner are notable in all images, but might be misinterpreted to be convex and not concave features – perception varies from person to person. Railway that makes a large curve in the North-South direction is clearly visible on all visualizations. Terraces in the village of Štanjel (upper centre of the image) are the most notable in a) and b). The same goes for the archaeological remains east from the village (round linear form). For the general terrain (right part of the image) the most appealing from the presented visualizations is SHD (a). On terraces in the rough terrain (upper right corner) SVF_d (d) shows more local detail than SHD and still provides enough general terrain clues. On the steep slopes facing away from the sun SVF_a (c) is too dark.

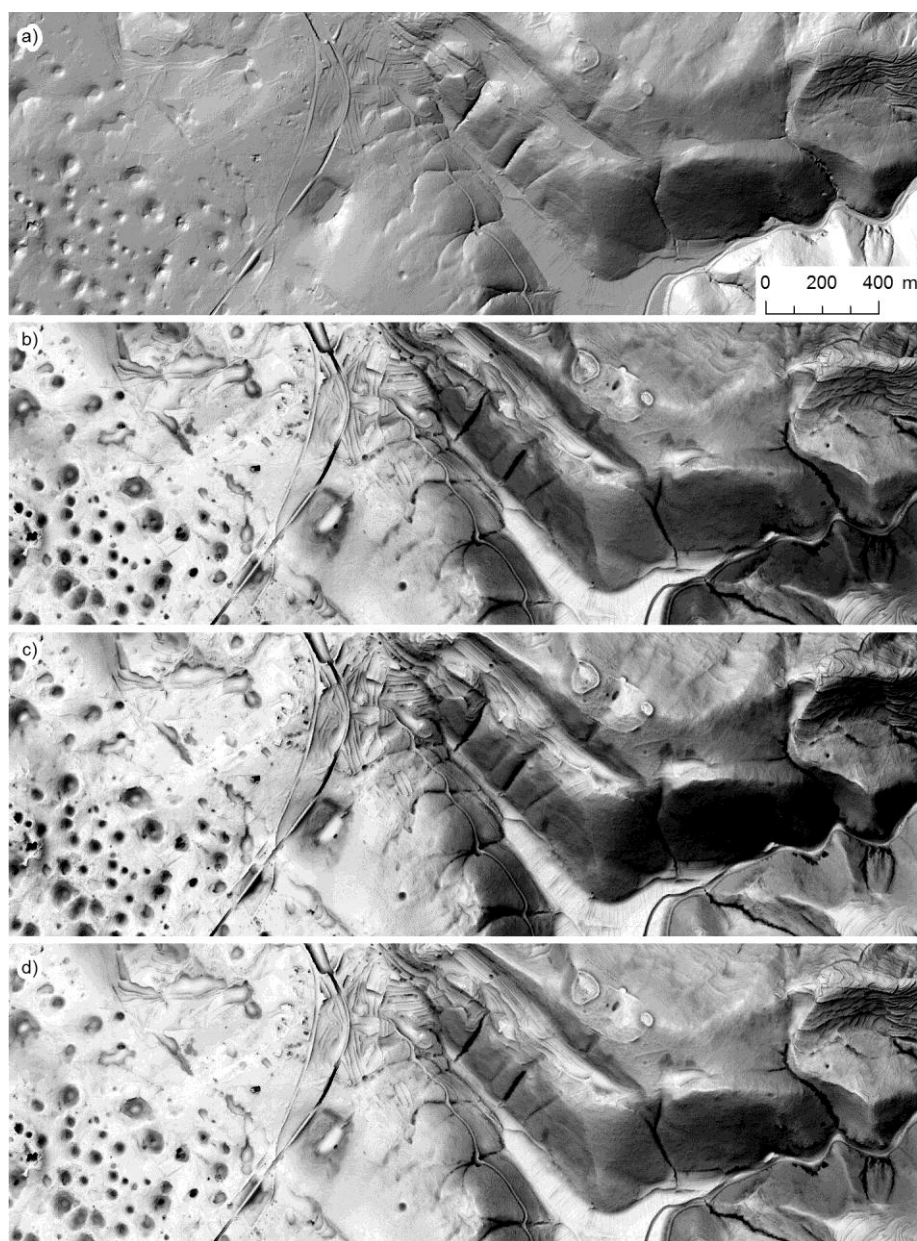


Fig. 7. A comparison between classical SHD (a) with linear stretch between 0.0 and 1.0, SVF (b), SVF_a (c), and SVF_d (d). All SVF based results are presented with linear stretch between 0.7 and 1.0. They were processed in 8 directions with maximum search radius 20 pixels (20 m). The area near Štanjel and Kobdilj (South-West Slovenia) covers an area of 3200×1100 m. The data source is lidar DEM of 1 m resolution.

Fig. 8 presents the comparison between image histograms (bin size of 0.01) of the data used for fig. 7. SHD has a smooth frequency function with modus just below 0.7 (this value corresponds to the cosine of the flat area using directional illumination source with elevation angle of $\varphi_s = 45^\circ$). Small local peak of the SHD curve (on the value of 0) shows that some saturated values were in the data. All three SVF based visualizations have significantly different histogram from the SHD histogram. Their modus is on the value of about 0.95 (such a value corresponds to mostly flat terrain with some small obstacles on the horizon). Because of high anisotropy characteristics of the illumination SVF_a has higher “left tail” of the frequency distribution; the values are transferred (comparing to SVF) from the middle part of the distribution to the left (low values) part of the distribution. This makes all South-Eastern slopes very dark. The distribution of SVF_d has even smaller range that makes it (using the same stretch parameter) in general brighter than the others.

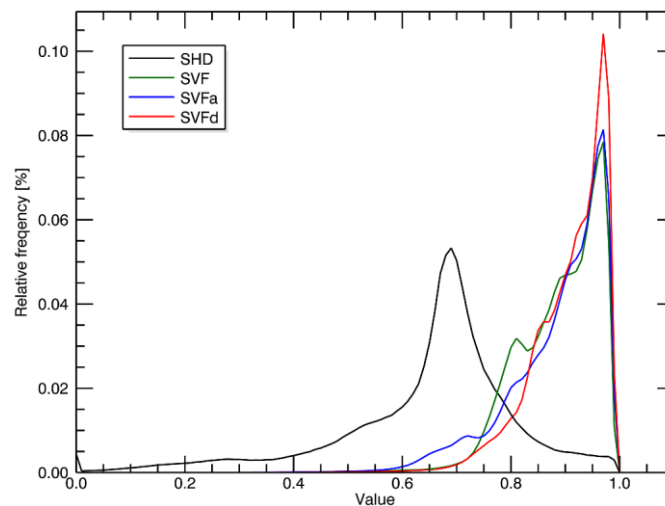


Fig. 8. A comparison between image histograms of data used in fig. 7.

The most significant outcome of the histogram comparison (fig. 8) is, however, the fact that the SVF based curves are not as smooth as SHD curve. This means that with these methods we can most likely identify more terrain features than with SHD. We also showed that the anisotropic diffuse illumination can enhance the terrain perception (figs. 4, 6, 7). The question remains: how far can we go by the anisotropy setup? Such a strong effect as we used in fig. 6 diminishes the advantages of diffuse over direct illumination because the shades (southern Alpine slopes) are too dark to expose any detail. These shades can be enhanced using an appropriate histogram manipulation. In the future we will thus continue our work with systematic study of parameters defining the illumination anisotropy models. We intend to define the most critical visualization parameter and its suitable values in order to make it easier to use for non-GIS experts. We also mentioned the importance of the histogram stretch. Here we always used only linear stretch in order to provide easier comparison between different visualizations. The appearance of the image can be significantly improved if an image stretch is optimized, thus this is the second object of our future work.

We can conclude that with introduction of anisotropic illumination it is in general possible to enhance the perception of the terrain illuminated by a diffuse light source, but it might be that the shades are too dark (the same problem as with the classical SHD). The proposed solutions can improve especially the interpretation of terrain data in hydrological analyses, enhance feature extraction, and are very suitable for visual validation of DEM geomorphologic quality. The two proposed methods result in slightly different visualizations, thus we suggest using SVF_a because it is faster and to easier to manipulate.

ACKNOWLEDGMENTS

The Centre of Excellence for Space Sciences and Technologies SPACE-SI is an operation partly financed by the European Union, European Regional Development Fund, and Republic of Slovenia, Ministry of Higher Education, Science and Technology.

The ASTER GDEM data were obtained through the online Data Pool at the NASA Land Processes Distributed Active Archive Center (LP DAAC), USGS/Earth Resources Observation and Science (EROS) Center, Sioux Falls, South Dakota (http://lpdaac.usgs.gov/get_data).

REFERENCES

- [1] Devereux, B.J., Amable, G.S. and Crow, P. (2008) Visualisation of LiDAR terrain models for archaeological feature detection. *Antiquity* 82, 470-479.
- [2] Gracia, A., Torres, J.L., De Blas, M., García, A. and Perez, R. (2011) Comparison of four luminance and radiance angular distribution models for radiance estimation. *Solar Energy* 85, 2202-2216.
- [3] Hobbs, K.F. (1999) An investigation of RGB multi-band shading for relief visualisation. *International Journal of Applied Earth Observation and Geoinformation* 1, 181-186.
- [4] Hobbs, K.F. (1995) The rendering of relief images from digital contour data. *The Cartographic Journal* 32, 111-116.
- [5] Horn, B.K.P. (1981) Hill shading and the reflectance map. *Proceedings of the IEEE* 69, 14-47.
- [6] Igawa, N., Koga, Y., Matsuzawa, T. and Nakamura, H. (2004) Models of sky radiance distribution and sky luminance distribution. *Solar Energy* 77, 137-157.
- [7] Imhof, E. (1982) *Cartographic relief presentation*. Berlin, New York, Walter de Gruyter.
- [8] Jarvis, A., Reuter, H.I., Nelson, A. and Guevara, E. (2008) Hole-filled seamless SRTM data V4, International Centre for Tropical Agriculture (CIAT). Available at: <http://srtm.csi.cgiar.org> [Accessed December 27, 2010].
- [9] Kennelly, P.J. and Stewart, A.J. (2006) A Uniform Sky Illumination Model to Enhance Shading of Terrain and Urban Areas. *Cartography and Geographic Information Science* 33, 21-36.
- [10] Kirk, R.L. et al. (2008) Ultrahigh resolution topographic mapping of Mars with MRO HiRISE stereo images: Meter-scale slopes of candidate Phoenix landing sites. *Journal of Geophysical Research* 113. Available at: <http://dx.doi.org/10.1029/2007JE003000>.
- [11] Li, D.H.W. and Cheung, G.H.W. (2005) Study of models for predicting the diffuse irradiance on inclined surfaces. *Applied Energy* 81, 170-186.
- [12] M., K. (2009) Sky luminance/radiance model with multiple scattering effect. *Solar Energy* 83, 1914-1922.
- [13] NASA Land Processes Distributed Active Archive Center (LP DAAC) at the USGS/Earth Resources Observation and Science (EROS) Center, Sioux Falls, South Dakota. (2003) ASTER Global DEM. Available at: <http://lpdaac.usgs.gov> [Accessed October 27, 2011].
- [14] Perez, R., Seals, R. and Michalsky, J. (1993) All-weather model for sky luminance distribution—Preliminary configuration and validation. *Solar Energy* 50, 235-245.
- [15] Yoëli, P. (1965) Analytische Schattierung. Ein kartographischer Entwurf. *Kartographische Nachrichten* 15, 141–148.
- [16] Yokoyama, R., Shirasawa, M. and Pike, R.J. (2002) Visualizing topography by openness: A new application of image processing to digital elevation models. *Photogrammetric Engineering and Remote Sensing* 68, 251-266.
- [17] Zakšek, K., Oštir, K. and Kokalj, Ž. (2011) Sky-View Factor as a Relief Visualization Technique. *Remote Sensing* 3, 398-415.
- [18] Zhukov, S., Inoes, A. and Kronin, G. (1998) An Ambient Light Illumination Model. In: *Rendering Techniques '98*: 45-56. Springer-Verlag Wien New York.